Research Square

Preprints are preliminary reports that have not undergone peer review.
They should not be considered conclusive, used to inform clinical practice,
or referenced by the media as validated information.

Transcriptomic and Metabolomic Responses of Botrytis cinerea Under L-Carvone Fumigation

Zhaoyu Ren
Xinyang Agriculture and Forestry University
Qisen Lu
Xinyang Agriculture and Forestry University
Chunling Yang
Xinyang Agriculture and Forestry University
Weichen You
Xinyang Agriculture and Forestry University
Chen Wang
Xinyang Agriculture and Forestry University
Yanan Zhi
Xinyang Agriculture and Forestry University
Lijun Chen
chlijun1980@163.com

Xinyang Agriculture and Forestry University

Article

Keywords: Botrytis cinerea, L-carvone, VOCs, RNA-seq, Metabolomic

Posted Date: August 31st, 2026

DOI: https://doi.org/10.21203/rs.3.rs-10642522/v1

License: This work is licensed under a Creative Commons Attribution 4.0 International License.
Read Full License

Additional Declarations: No competing interests reported.

Version of Record: A version of this preprint was published at Scientific Reports on November 4th, 2026.
See the published version at https://doi.org/10.1038/s41598-026-78382-9.

Transcriptomic and Metabolomic Responses of *Botrytis cinerea* Under L-Carvone Fumigation

Zhaoyu Ren[1,2], Qisen Lu[1,2], Chunling Yang[1,2], Weichen You[1,2], Chen Wang[1], Yanan Zhi[1,2], Lijun Chen[1,2*]

[1]Xinyang Agriculture and Forestry University, Xinyang 464000, China.

[2]Xinyang Key Laboratory of Functional Volatiles Resources for Plant Protection, Xinyang 464000, China

Corresponding author：Prof. Chen Lijun. E-mail: chlijun1980@163.com

Abstract: *Botrytis cinerea*, a necrotrophic phytopathogenic fungus with a wide host range, causes severe postharvest gray mold and huge economic losses worldwide. Conventional chemical fungicides easily induce multidrug resistance in field isolates, while the natural monoterpene volatile L-carvone exhibits broad-spectrum antifungal activity. However, the comprehensive molecular mechanism by which L-carvone suppresses *B. cinerea* remains unclear. In this study, mycelia of *B. cinerea* were treated with L-carvone at EC_{50} concentration with sterile water as blank control. RNA-seq transcriptome and HS-SPME-GC-MS untargeted metabolome sequencing were performed to systematically dissect molecular responses via integrated omics analysis. A total of 1,531 DEGs were identified, including 347 upregulated and 1,184 downregulated genes. Upregulated DEGs were enriched in sulfur metabolism, cysteine and methionine metabolism involved in transient antioxidant response, whereas downregulated DEGs mainly participated in cell membrane lipid biosynthesis, carbon energy metabolism, phytotoxin synthesis and conidiation. A total of 246 DAMs were screened. Antioxidant terpenoids including γ-cadinene, carvacrol and camphene were significantly accumulated, while lipid precursors for cell membrane assembly and toxic botrydial-derived aldehydes were drastically reduced. L-carvone simultaneously blocked phytotoxin biosynthesis, ergosterol membrane formation, vegetative growth and asexual reproduction of *B. cinerea*. The fungus only activated short-term ROS scavenging and xenobiotic efflux pathways, whereas the long-term glutathione-dependent antioxidant system was suppressed, leading to irreversible oxidative damage. This study reveals the multi-target antifungal mechanism of L-carvone at transcriptional and metabolic levels, providing theoretical support for green control of gray mold and the development of botanical fungicides with novel modes of action.

Key words: *Botrytis cinerea*, L-carvone, VOCs, RNA-seq, Metabolomic

Introduction

Botrytis cinerea is a necrotrophic phytopathogenic fungus capable of infecting more than 1,400 plant species and causing gray mold, ranking among the most destructive plant pathogens worldwide[1,2]. The pathogen inflicts severe damage during crop growth and postharvest storage, resulting in global economic losses approaching USD 100 billion annually. *B. cinerea* possesses sophisticated pathogenicity mechanisms and secretes multiple virulence factors including cell wall-degrading enzymes, growth regulators, phytotoxins, reactive oxygen species (ROS), oxalic acid and plant immune suppressors to facilitate host infection[3]. For decades, gray mold management has heavily depended on conventional synthetic fungicides[4]. However, *B. cinerea* features short reproduction cycles, massive spore production and rapid genetic variation, making it a pathogen with a high risk of fungicide resistance[5]. Under persistent chemical selection pressure, field isolates of *B. cinerea* have developed severe single and multi-drug resistance to nearly all mainstream fungicides, including benzimidazoles, dicarboximides and succinate dehydrogenase inhibitors, which drastically reduces field control efficacy[6]. Therefore, exploring novel bio-based antifungal molecules and developing chemical-free green control strategies is of great practical significance.

Plant volatile organic compounds (VOCs), endogenous secondary metabolites, exert potent inhibitory effects on diverse phytopathogenic fungi. Terpenoid VOCs suppress fungal viability via multiple modes of action, including disrupting cell membrane integrity, disturbing intracellular redox homeostasis, inhibiting spore germination and hyphal growth, and downregulating virulence-related gene expression[7-9].

Glucosinolate breakdown VOCs released by Brassicaceae plants inhibit *B. cinerea* growth and elucidated the molecular mechanism whereby transporter proteins mediate fungal tolerance to VOC stress[10]. *Origanum vulgare* essential oil and its dominant constituent carvacrol exert strong growth suppression against *B. cinerea* via disrupting membrane integrity, triggering cytoplasmic leakage and excessive ROS accumulation; carvacrol exhibits far higher antifungal efficiency than thymol and

crude oregano oil[11]. Terpenoid volatiles from lemongrass, thyme and oregano essential oils damage the cell membrane of *B. cinerea* and effectively reduce gray mold incidence in strawberry fruits[12]. In underground ecosystems, root-emitted volatile terpenes and aldehydes suppress soil-borne pathogens such as *Fusarium* spp. and *Rhizoctonia solani*, and VOC fumigation reshapes soil pathogenic fungal communities[13].

Blends of essential oil VOCs strongly inhibit multiple postharvest brown rot pathogens including *Monilinia fructicola*, which are more sensitive to terpenoid volatiles than *B. cinerea*[14]. Beyond direct antagonism against pathogens, certain alcohol and ester VOCs can activate host defense pathways and enhance fruit resistance to gray mold[15]. L-carvone, a natural monoterpene VOC, exhibits broad-spectrum antifungal activity and high volatility. It embeds into the phospholipid bilayer of fungal cell membranes to impair membrane fluidity and integrity, increase membrane permeability and trigger intracellular leakage; it also induces massive ROS accumulation, disrupts biofilm formation and suppresses germ tube development[16]. Compared with phenolic volatiles such as carvacrol and thymol, L-carvone causes less irritation and exhibits superior gas-phase diffusion stability, making it more suitable for closed fumigation control[17]. Previous study evaluated the antifungal activity of five VOCs against multiple phytopathogens and found that carvone inhibits mycelial growth of *Fusarium* spp. in a dose-dependent manner[18]. Carvone fumigation disrupts membrane structure and mitochondrial function to suppress the growth of *B. cinerea*, *Penicillium expansum* and *Monilinia fructicola*, and significantly alleviates postharvest gray mold of fruits and vegetables[11]. L-carvone inhibits vegetative growth and asexual reproduction of *B. cinerea*, damages membrane structure and physiological function, induces irreversible oxidative injury and attenuates fungal virulence[18]. Previous studies have validated the antifungal efficacy of carvone, yet they are limited to superficial physiological indicators such as colony growth, membrane damage and oxidative stress, without clarifying the comprehensive molecular mechanism underlying carvone-mediated inhibition of fungal viability.

In the present study, integrated transcriptome and metabolome profiling was performed to characterize molecular alterations in *B. cinerea* under L-carvone stress. This study aims to elucidate the molecular mechanism by which L-carvone suppresses growth and virulence of *B. cinerea*, advance the understanding of antibacterial mechanisms of natural monoterpenoids, and provide a theoretical foundation for developing botanical fungicides with novel modes of action.

Materials and Methods

Fungal culture and sample preparation

The *Botrytis cinerea* strain used in this study was isolated and preserved by the Laboratory of Plant Pathology, College of Agronomy, Xinyang Agriculture and Forestry University. Standard L-carvone (Aladdin Biochemical Technology Co., Ltd., Shanghai, China) was stored at 4 °C.

B. cinerea were cultured on PDA medium for 3–4 d, followed by treatment with L-carvone at the EC_{50} concentration and continuous dark incubation at 25 °C for another 3–4 d. Sterile distilled water treatment served as the blank control group (BCCK), while the L-carvone treatment group was designated BCEC. Three biological replicates were set for transcriptome sequencing, and five biological replicates for metabolome sequencing. Mycelial samples from the control and treatment groups were collected into pre-cooled 1.5 mL centrifuge tubes, snap-frozen in liquid nitrogen and stored at −80 °C.

RNA extraction and strand-specific RNA library preparation

Total RNA was extracted using the mirVana miRNA Isolation Kit (Ambion) following the manufacturer's protocol. RNA integrity was evaluated using an Agilent 2100 Bioanalyzer (Agilent Technologies, Santa Clara, CA, USA). The samples with an RNA integrity number (RIN) ≥ 7 were subjected to subsequent analysis. The libraries were constructed using the TruSeq Stranded mRNA LT Sample Prep Kit (Illumina, San Diego, CA, USA) according to the manufacturer's protocol. These libraries were then sequenced on the Illumina sequencing platform (HiSeq 2000), and 125 bp/150 bp paired-end reads were generated.

Quality control and mapping

Transcriptome sequencing and analysis were conducted by Yuanxin Biomedical Co., Ltd. (Shanghai, China). The raw reads were processed using Trimmomatic[19]. The reads containing poly-N and low-quality reads were removed to obtain clean reads. The clean reads were then mapped to the reference genome (B05.10) using HISAT2[20].

Gene-level and transcript-level quantification, analysis of differentially expressed genes (DEGs), cluster analysis, GO and KEGG enrichment

Gene expression levels were quantified as FPKM values using StringTie software. Significantly differentially expressed genes (DEGs) were identified using the estimateSizeFactors and nbinomTest functions in the DESeq package (2012)[21]. Genes with $|\log_2 FC| > 1$ and FDR < 0.05 were defined as DEGs. DEGs were annotated against the GO and KEGG databases[22-24], and hypergeometric tests were applied to identify significantly enriched functional pathways. Hierarchical clustering of DEGs was performed to visualize gene expression patterns. GO and KEGG pathway enrichment analyses of DEGs were implemented in R based on hypergeometric distribution[25]. For transcript-level quantification, read counts and FPKM values of protein-coding transcripts were calculated using Bowtie2[26] and eXpress[27].

Metabolome sequencing

Volatile metabolites were extracted via headspace solid-phase microextraction (HS-SPME). Desorption of volatile organic compounds was conducted at the GC inlet (Agilent 8890) under splitless mode at 250 °C for 5 min. Metabolite identification and quantification were performed using GC-MS (Agilent 8890/7000D) equipped with a DB-5ms capillary column (30 m × 0.25 mm × 0.25 μm). Helium was used as carrier gas at a constant linear velocity of 1.2 mL/min. The temperature program was set as follows: hold at 40 °C for 3.5 min, ramp to 100 °C at 10 °C/min, ramp to 180 °C at 7 °C/min, ramp to 280 °C at 25 °C/min, and hold at 280 °C for 5 min. Mass spectra were acquired under electron ionization (EI) mode at 70 eV. The quadrupole mass detector, ion source and transfer line were maintained at 150 °C, 230 °C and 280 °C, respectively. Selected ion monitoring (SIM) mode was adopted for metabolite identification and quantification.

Metabolome data analysis

Metabolite data from the BCCK and BCEC groups were normalized, followed by principal component analysis (PCA) implemented via the prcomp function in base R (v4.1.2). Orthogonal projections to latent structures-discriminant analysis (OPLS-DA) was performed using the R package MetaboAnalystR (v1.0.1). Metabolites satisfying VIP > 1, $|\log_2 FC| \geq 1.0$ and P-value < 0.05 were defined as significantly differential abundant metabolites (DAMs). All annotated metabolites were mapped to the KEGG Compound database and subsequently linked to the KEGG Pathway database[22-24]. Metabolite set enrichment analysis (MSEA) was conducted, and hypergeometric tests were used to determine the statistical significance of enriched metabolite sets.

Results

Transcriptome profiling of RNA-Seq data

Raw RNA-seq reads were quality-filtered to remove empty reads, adapter sequences and low-quality sequences, generating a total of 69.67 GB clean data. For the BCCK group, the average clean reads and clean bases were 78.80 million and 11.40 Gb, respectively, with an average error rate of 0.03%, mapping rates ranging from 96.00% to 96.22%, and Q30 values between 93.24% and 93.38%. For the BCEC group, the average clean reads and clean bases reached 81.57 million and 11.82 Gb, with an average error rate of 0.03%, mapping rates from 96.34% to 96.53%, and Q30 values ranging from 93.41% to 93.50% (Table 1). These results indicated low base error rates, high mapping ratios and high Q30 values across both groups, confirming qualified sequencing data for subsequent transcriptome analysis.

Sequencing saturation curves were plotted to evaluate the reliability of gene detection under different sequencing depths, as genes with high expression levels reach saturation more readily than low-expression transcripts. The average total number of detected genes was 13,199 in the BCCK group and 13,062 in the BCEC group (Fig. S1).

Gene expression boxplots based on $\log_2(FPKM + 1)$ illustrated global transcript distribution patterns across samples. The median and interquartile ranges of gene expression were consistent within biological replicates of each group, while obvious

shifts were observed between groups, indicating reliable biological reproducibility and altered transcriptional profiles of *B. cinerea* under L-carvone stress (Fig. 1a). Sample correlation heatmaps revealed high correlation coefficients within groups and low correlation coefficients between groups (Fig. 1b). PCA showed complete separation of samples from distinct treatments, with PC1 and PC2 explaining 56.17% and 24.93% of total transcriptional variation, respectively (Fig. 1c). Collectively, these results demonstrated that L-carvone drastically reshapes the transcriptome of *B. cinerea*. Using the thresholds $|\log_2 FC| > 1$ and FDR < 0.05, a total of 1,531 DEGs were identified, consisting of 347 upregulated and 1,184 downregulated genes (Table S1). The number of downregulated DEGs was approximately 3.4-fold higher than upregulated DEGs (Fig. 1d), suggesting global transcriptional suppression of *B. cinerea* upon L-carvone exposure. Hierarchical clustering of all DEGs revealed highly consistent expression patterns among the three biological replicates within each group (Fig. 2).

Functional Enrichment of DEGs via KEGG and GO Analysis

KEGG enrichment revealed that upregulated DEGs were significantly enriched in global metabolic pathways, sulfur metabolism, and cysteine and methionine biosynthesis (Fig. 3a). Sulfur metabolism and cysteine/methionine metabolism constitute the core antioxidant and detoxification network of *B. cinerea* against exogenous stress; these pathways are transcriptionally activated to eliminate intracellular ROS and alleviate oxidative damage under terpenoid VOC stress[10,28]. Downregulated DEGs were predominantly enriched in starch and sucrose metabolism, glycerolipid metabolism, peroxisome biogenesis and amino acid biosynthesis (Fig. 3b). Inhibition of carbon metabolism restricts energy supply for fungal growth; impaired glycerolipid metabolism blocks membrane lipid biosynthesis and compromises membrane integrity; suppressed peroxisome biogenesis weakens long-term antioxidant capacity[11,29]. In summary, L-carvone triggers rapid activation of emergency defense pathways in *B. cinerea*, while core pathways supporting vegetative growth, energy metabolism and membrane biogenesis remain persistently repressed.

GO functional enrichment showed that upregulated DEGs were significantly enriched in oxidoreductase activity, cofactor binding and catalytic activity (Fig. 4a). Induction of oxidoreductase genes reflects activation of antioxidant and detoxification machinery to counteract L-carvone stress[30]. Downregulated DEGs were highly enriched in plasma membrane, transmembrane transporter activity and membrane component terms (Fig. 4b), demonstrating severe impairment of membrane structure and transmembrane transport functions[11].

Analysis of Key Significantly Differentially Expressed Genes

Key genes involved in phytotoxin biosynthesis, damage repair and vegetative development were summarized in Table 2. The master transcription factor for botrydial biosynthesis *BcBOT6*, along with key biosynthetic enzyme genes *BcBOT1* and *BcBOT2*[31-34], cell wall-degrading enzyme genes *Bcpg1*, *Bcpg2* and *Bccel1*[35-38], and conidiation regulatory genes *Bccon1* and *Bccon2*[39-41] were all significantly downregulated. These results indicated that L-carvone blocks botrydial synthesis, suppresses host cell wall degradation and asexual reproduction, and markedly attenuates fungal virulence.

For oxidative stress response, long-term detoxification genes including the rate-limiting glutathione synthesis gene *Bcmet16*, glutathione synthetase *BcGCL* and glutathione peroxidase *BcGPX* were significantly repressed[30,42,43]. In contrast, genes responsible for transient ROS scavenging and xenobiotic efflux, including *BcSOD1*, *BcCAT1*, *BcGST1* and *BcatrO*, were significantly upregulated[30,42,44]. This pattern indicated that *B. cinerea* can only initiate short-term emergency responses to eliminate ROS and extrude terpenoid compounds, lacking sustained capacity to resist persistent oxidative injury.

Genes essential for vegetative development, including ergosterol biosynthetic genes *BcERG7*, *BcERG12*, *BcERG27*, fatty acid synthase *BcFAS1*[45], cytoskeletal genes *BcactA*[46] and *BcTUB1*[47], and polar hyphal growth GTPase *BcCDC42*[48], were uniformly downregulated. By contrast, cell wall repair genes *Bcchs1* and *BcFKS* were slightly upregulated[38,49,50]. This transcriptional shift revealed that carbon and sulfur

metabolic resources are redirected toward stress response, severely limiting membrane biogenesis, hyphal elongation and conidiation.

Metabolome Profiling and Global Sample Differentiation

Metabolite composition analysis provides an intuitive overview of global metabolite distribution across samples. Overlapping total ion chromatograms (TICs) of QC samples confirmed stable mass spectrometry detection signals (Fig. S2). Global metabolite classification revealed that metabolites of *B. cinerea* were primarily composed of hydrocarbons, heterocyclic compounds and lipids (Fig. 5). PCA was performed to assess global metabolic variation between groups. PC1 and PC2 explained 56.85% and 11.72% of total metabolic variance, respectively. Samples from BCEC and BCCK groups formed distinct clusters without overlap, with tight aggregation within each group reflecting excellent biological reproducibility (Fig. 6a). OPLS-DA results were consistent with PCA observations (Fig. 6b), collectively verifying that L-carvone drastically remodels the metabolome of *B. cinerea*.

DAMs were screened using the criteria $0.5 \leq$ fold change ≤ 2, P-value < 0.05 and VIP $>$ 1. A total of 306 metabolites showed no significant abundance changes, while 246 metabolites were identified as DAMs (Table S2), including 166 significantly upregulated and 80 significantly downregulated metabolites (Fig. 7a). Hierarchical clustering heatmaps of DAMs showed clear separation between BCEC and BCCK groups with consistent metabolite profiles within replicates (Fig. 7a), confirming profound metabolic reprogramming triggered by L-carvone fumigation.

KEGG Pathway Enrichment of DAMs

All 246 annotated DAMs were mapped to the KEGG database for pathway enrichment analysis. DAMs were predominantly enriched in phenylalanine metabolism and biosynthesis of secondary metabolites, two core pathways mediating resistance to exogenous antifungal agents and oxidative damage in *B. cinerea*[33]. Coenzyme biosynthesis pathways were also significantly enriched (Fig. 8). Upregulation of cofactor and mitochondrial antioxidant precursor metabolism indicated global perturbation of cellular redox networks and altered substrate supply for oxidoreductase reactions[51]. These metabolomic results demonstrated that

L-carvone mainly targets secondary metabolism and redox homeostasis modules in *B. cinerea*.

Analysis of Key Significantly Differential Abundant Metabolites

Key DAMs associated with phytotoxin biosynthesis, stress damage repair and vegetative development were summarized in Table 3. Under L-carvone stress, the core toxic unsaturated aldehydes trans,trans-2,4-decadienal and (E)-2-octenal[43,52] were significantly reduced, while phytotoxin precursors including 4-hydroxybenzoic acid, phenylacetic acid and decanal accumulated as compensatory intermediates[32,37]. Inhibition of toxic aldehyde synthesis has been reported in *B. cinerea* treated with benzothiazole, which interferes with central carbon metabolism and suppresses toxin precursor production to retard hyphal growth and virulence[53]. Consistent with this previous report, benzothiazole was significantly accumulated in the BCEC group. Antioxidant metabolites including γ-cadinene, carvacrol, camphene and dipropyl disulfide[30,43,52,54,55], as well as the membrane repair metabolite 1-methyl-4-(1-methylethyl)cyclohexanol, were markedly upregulated, revealing the metabolic response of *B. cinerea* to L-carvone-induced oxidative stress and membrane injury. In contrast, lipid precursors essential for cell membrane biogenesis and conidiation, namely (1-methylethylidene)cyclohexane and 3,7,7-trimethylbicyclo[4.1.0]heptane, were significantly depleted[37,45,52]. Meanwhile, metabolites supporting amino acid synthesis and cell wall maintenance, including (2,2,6-trimethylbicyclo[4.1.0]hept-1-yl)methanol, 1,2,3,5-tetramethylbenzene and biphenyl, were accumulated as compensatory metabolites[36,37,52,56]. These metabolic shifts demonstrated that L-carvone disrupts central carbon metabolism of *B. cinerea*, redirecting metabolic flux from vegetative growth and development toward stress defense.

Discussion

The necrotrophic pathogen *Botrytis cinerea* possesses a broad host range and frequently causes destructive gray mold outbreaks under low-temperature postharvest storage conditions, leading to massive postharvest economic losses via secretion of necrogenic phytotoxins[1,57]. Reliance on chemical fungicides has selected for

multi-cross resistant field isolates with persistent loss of control efficacy; additionally, fungicide residues accumulate along food chains and disrupt fruit and vegetable microecology, posing severe threats to ecological safety and human health[10,58]. Plant terpenoid volatile oils exhibit unique advantages including zero residual risk and multi-target antifungal activity, simultaneously disrupting fungal membrane synthesis, intracellular redox homeostasis and phytotoxin metabolism, making them ideal eco-friendly alternatives to synthetic fungicides[7,8]. Previous physiological studies confirmed that food-grade L-carvone suppresses vegetative growth and asexual reproduction of *B. cinerea*, damages membrane structure and physiological function, induces irreversible oxidative injury and attenuates fungal virulence[9]. Herein, integrated RNA-seq and metabolome analyses systematically characterized the inhibitory mechanism of L-carvone from three perspectives: phytotoxin biosynthesis, stress damage repair and vegetative growth, providing empirical evidence for developing novel botanical fungicides.

RNA-seq generated a total of 69.67 GB clean data and revealed global transcriptional remodeling in L-carvone-treated *B. cinerea*, with 347 upregulated and 1,184 downregulated DEGs (Fig. 1; Table S1), confirming overall transcriptional suppression of fungal growth. Hierarchical clustering of DEGs verified highly consistent transcriptional profiles within biological replicates of each group (Fig. 2). KEGG enrichment demonstrated that upregulated DEGs were enriched in sulfur metabolism and cysteine/methionine biosynthesis for transient ROS clearance[10,30], whereas downregulated DEGs were enriched in carbon energy metabolism, glycerolipid biosynthesis and peroxisome pathways essential for sustained growth and membrane integrity[11,29]. These transcriptional patterns are consistent with the molecular responses of *B. cinerea* exposed to tea tree oil and aldehyde volatiles[33,46]. GO annotation revealed enrichment of oxidoreductase, cofactor binding and catalytic activity among upregulated DEGs (Fig. 4a), while downregulated DEGs were overrepresented in plasma membrane, transmembrane transport, extracellular region, hydrogen peroxide metabolism and secondary biosynthetic processes (Fig. 4b).

Widespread repression of membrane and transport-related genes confirmed severe impairment of membrane biogenesis and nutrient translocation.

Metabolome profiling indicated that global metabolites of *B. cinerea* were dominated by hydrocarbons, heterocyclic compounds and lipids (Fig. 5). PCA and OPLS-DA collectively confirmed profound metabolic shifts upon L-carvone exposure (Fig. 6). A total of 246 DAMs were identified, comprising 166 upregulated and 80 downregulated metabolites (Fig. 7a), and hierarchical clustering validated distinct metabolic signatures between treatment and control (Fig. 7b). KEGG enrichment of DAMs highlighted secondary metabolism and redox pathways as primary targets of L-carvone, consistent with transcriptome observations (Fig. 8).

Botrydial, a sesquiterpenoid phytotoxin that induces host necrosis, relies on the bipartite biosynthetic cluster transcriptionally controlled by the $Zn(II)_2Cys_6$ transcription factor *BcBOT6*; *BcBOT2* catalyzes core skeleton cyclization and *BcBOT1* mediates oxidative modification, and loss of any of these genes drastically reduces necrogenic virulence[33,59]. Transcriptome data showed significant downregulation of *BcBOT1*, *BcBOT2* and *BcBOT6* under L-carvone stress. Metabolome analysis revealed depletion of mature toxic aldehyde derivatives trans,trans-2,4-decadienal and (E)-2-octenal, despite mild accumulation of aromatic and aliphatic toxin precursors including 4-hydroxybenzoic acid, phenylacetic acid and decanal. Blockage of downstream oxidative modification prevents complete maturation of toxic aldehydes[32]. Moreover, cell wall-degrading enzyme genes *Bcpg1*, *Bcpg2* and *Bccel1* were significantly repressed[35-38]. Combined transcriptomic and metabolomic evidence demonstrated that L-carvone simultaneously blocks two core virulence pathways: phytotoxin biosynthesis and host cell wall penetration.

Terpenoid volatile exposure triggers massive ROS burst in *B. cinerea*, which activates two distinct antioxidant systems: short-term emergency detoxification and long-term glutathione-dependent defense[43,60]. Transcriptome data showed significant induction of *BcSOD1*, *BcCAT1*, *BcGST1* and *BcatrO*, which mediate instantaneous ROS scavenging and extracellular efflux of xenobiotics to mitigate acute oxidative damage[42,44]. However, key genes governing sulfur assimilation and glutathione

synthesis (*Bcmet16*, *BcGCL*, *BcGPX*) were uniformly repressed. *Bcmet16* catalyzes rate-limiting sulfate reduction for cysteine and glutathione production; *BcGCL* encodes the rate-limiting enzyme for glutathione biosynthesis; *BcGPX* utilizes reduced glutathione to detoxify lipid peroxides. Collectively, these three genes constitute a sustained antioxidant barrier repairing membrane lipid oxidation[43]. Persistent suppression of this pathway eliminates long-term antioxidant capacity, leading to cumulative irreversible lipid peroxidation.

Ergosterol, a unique sterol in fungal membranes essential for fluidity, barrier function and transmembrane transport, represents a canonical target of monoterpenoid compounds[30,61]. All three core ergosterol biosynthetic genes *BcERG7*, *BcERG12* and *BcERG27* were transcriptionally repressed, accompanied by drastic depletion of upstream terpenoid precursors (1-methylethylidene)cyclohexane and 3,7,7-trimethylbicyclo[4.1.0]heptane in the metabolome, confirming direct inhibition of sterol biosynthesis by L-carvone. Following membrane damage, *B. cinerea* redirects global carbon flux toward compensatory cell wall reinforcement. Transcript upregulation of chitin synthase *Bcchs1* and glucan synthase *BcFKS* corresponded to elevated metabolites (2,2,6-trimethylbicyclo[4.1.0]hept-1-yl)methanol, 1,2,3,5-tetramethylbenzene and biphenyl, which participate in polysaccharide cross-linking to thicken the outer cell wall and reduce xenobiotic penetration[36,37]. Nevertheless, cell wall chitin and glucan only form the outer structural layer and cannot compensate for membrane leakage and organelle injury caused by ergosterol deficiency, ultimately leading to retarded hyphal growth and drastically reduced conidiation. Transcriptional repression of conidiation markers *Bccon1* and *Bccon2* further validated this phenotypic outcome[39,40].

Actin and microtubules form the fungal cytoskeleton, supporting hyphal elongation, vesicular trafficking and conidiation; impaired cytoskeleton biosynthesis results in abnormal hyphal morphology and growth arrest[46-48]. In this study, cytoskeletal genes *BcactA*, *BcTUB1* and polar growth GTPase *BcCDC42* were all significantly downregulated, revealing the molecular basis of L-carvone-mediated growth suppression in *B. cinerea*.

In conclusion, integrated transcriptome and metabolome analyses demonstrated that L-carvone simultaneously suppresses phytotoxin biosynthesis, membrane lipid metabolism and vegetative reproduction of *B. cinerea*, resulting in attenuated fungal growth and virulence. This study provides multi-omics evidence elucidating the multi-target antifungal mechanism of L-carvone and lays a theoretical foundation for integrated green control of gray mold disease.

Data availability

All raw sequencing data have been submitted to the NCBI Sequence Read Archive (SRA) database under the accession numbers SRX34795505-SRX34795510. (https://www.ncbi.nlm.nih.gov/sra/PRJNA1512637).

Contributions

ZR: Conceptualization, Data curation, Formal analysis, Investigation, Writing-original draft, Writing-review & editing. QL: Methodology, Software, Validation, Visualization, CY: Conceptualization, Supervision, Visualization. WY: Conceptualization, Validation. CW: Methodology, Software. YZ: Validation, Visualization. LC: Methodology, Funding acquisition, Supervision, Writing-review & editing.

Funding

This work was supported by Natural Science Foundation of Henan Province (Grant No. 232300420030) and Key Research Project of Henan Provincial Universities (Grant No. 25B210017).

Ethics declarations

Ethics, Consent to Participate, and Consent to Publish declarations

Not applicable.

Competing Interest

The authors declare that they have no conflicts of interest.

Reference

1. Dean, R. Van Kan, J.A.L. Hammond-Kosack, K.E.; Di Pietro, A.; Spanu, P.D.; Rudd, J.J.; Dickman, M.B.; Kahmann, R.; Ellis, J.G.; Foster, G.D. The top 10 fungal pathogens in molecular plant pathology. *Mol. Plant Pathol.* **2012**, 13, 414–430.
2. Dwivedi, M.; Singh, P.; Pandey, A.K. Botrytis fruit rot management: what have we achieved so far?. *Food Microbiol.* **2024**, 122, 104564.
3. Wang, K.C.; Li, Z.B.; Shen, X. Terpinen-4-ol triggers autophagy activation and metacaspase-dependent apoptosis against *Botrytis cinerea*. *Front. Microbiol.* **2025**, 16, 1600831.
4. Rosslenbroich, H.; Stuebler, D. *Botrytis cinerea* — history of chemical control and novel fungicides for its management. *Crop Prot.* **2000**, 19, 557–571.
5. Khan, A.R.; Ali, Q.; Ayaz, M. Bio-perfume guns: antifungal volatile activity of *Bacillus* sp. LNXM12 against postharvest pathogen *Botrytis cinerea* in tomato and strawberry. *Pestic. Biochem. Physiol.* **2024**, 203, 105995.
6. Shao, W.; Zhao, Y.; Ma, Z. Advances in understanding fungicide resistance in *Botrytis cinerea* in China. *Phytopathology* **2021**, 111, 455–463.
7. Álvarez-García, S.; Moumni, M.; Romanazzi, G. Antifungal activity of volatile organic compounds against *Botrytis cinerea*, *Monilinia fructicola*, *Monilinia laxa*. *Front. Plant Sci.* **2023**, 14, 1274770.
8. Kgang, I.E.; Klein, A.; Mohamed, G.G.; Mathabe, P.M.; Belay, Z.A.; Caleb, O.J. Enzymatic and proteomic exploration into the inhibitory activities of lemongrass and lemon essential oils against *Botrytis cinerea*. *Front. Microbiol.* **2023**, 13, 1101539.
9. Olim, S.; Kutywayo, D.; Chikwambi, Z. Microbial volatile organic compounds: insights into plant defence. *Plants* **2024**, 13, 2013.
10. Vela-Corcía, D.; Vicedo, B.; Flors, V. An MFS transporter from *Botrytis cinerea* provides tolerance to glucosinolate-breakdown products and is required for full pathogenicity. *Nat. Commun.* **2019**, 10, 2888.

11. Liu, Y.; Wang, H.; Wei, Y. Effects of *Origanum vulgare* essential oil and its two main components, carvacrol and thymol, on the plant pathogen *Botrytis cinerea*. *PeerJ* **2020**, 8, e9626.
12. Yan, J.Q.; Li, Y.; Zhang, H. Antifungal activities and mode of action of *Cymbopogon citratus*, *Thymus vulgaris*, and *Origanum heracleoticum* essential oil vapours against *Botrytis cinerea*. *Foods* **2021**, 10, 2451.
13. Delory, B.; Delaplace, P.; Fauconnier, M.L. Volatile organic compounds shape belowground plant–fungi interactions. *Front. Plant Sci.* **2022**, 13, 914792.
14. Chen, L.; Wang, X.; Liu, J. Investigating the action model of resistance enhancement induced by bacterial volatile organic compounds against *Botrytis cinerea* in tomato fruit. *Front. Plant Sci.* **2024**, 14, 1475416.
15. Bouyahya, A.; Mechchate, H.; Benali, T.; et al. Health benefits and pharmacological properties of carvone. *Biomolecules* **2021**, 11, 1803.
16. Terzi, V.; Morcia, C.; Malnati, M. In vitro antifungal activity of terpinen-4-ol, eugenol, carvone, 1,8-cineole and thymol against mycotoxigenic plant pathogens. *Food Addit. Contam. Part A* **2012**, 29, 415–422.
17. Liu, Y.H.; Yuan, T.T.; Chen, T.; Li, B.Q.; Tian, S.P. Carvone fumigation suppresses postharvest fruit diseases by disturbing mitochondrial function and impairing membrane integrity. *Postharvest Biol. Technol.* **2025**, 230, 113810.
18. Zhi, Y.N.; You, W.C.; Li, Y.; Li, Y.H.; Wang, C.S.; Chen, L.J. Preliminary investigation of the fumigation antifungal activity and mechanisms of L-carvone. *Plant Prot.* **2025**, 51, 63–71.
19. Li, B.; Duan, W.; Lin, G.; Ma, X.; Wen, R.; Zhang, Z. An effective and promising strategy for plant protection: synthesis of L-carvone-based thiazolinone–hydrazone/nanochitosan complexes. *Int. J. Mol. Sci.* **2025**, 26, 11086.
20. Su, Y.; Miao, W.; Wang, C.; Jin, Z.; Duan, T.; Wang, C.W. Multifaceted antifungal mechanisms of volatile organic compounds emitted by *Pseudomonas chlororaphis* strain ZL3 against *Botrytis cinerea*. *Microbiol. Spectr.* **2025**, 13, e02706-24.

21. Song, G.; Du, S.; Sun, H. Antifungal mechanism of (E)-2-hexenal against *Botrytis cinerea* growth revealed by transcriptome analysis. *Front. Microbiol.* **2022**, 13, 951751.
22. Siewers, V.; Viaud, M.; Jimenez-Teja, D. Functional analysis of the cytochrome P450 monooxygenase gene *bcbot1* of *Botrytis cinerea* indicates that botrydial is a strain-specific virulence factor. *Mol. Plant-Microbe Interact.* **2005**, 18, 602–612.
23. Dalmais, M.; Schumacher, J.; Moraga, J. The *Botrytis cinerea* phytotoxin botcinic acid requires two polyketide synthases for production and has a redundant role in virulence. *Mol. Plant Pathol.* **2011**, 12, 564–579.
24. Porquier, A.; Morgant, G.; Moraga, J.; Dalmais, B.; Luyten, I.; Simon, A.; Pradier, J.M.; Amselem, J.; Viaud, M.; Collado, I.G. The botrydial biosynthetic gene cluster of *Botrytis cinerea* displays a bipartite genomic organization and is positively regulated by the putative $Zn(II)_2Cys_6$ transcription factor BcBot6. *Fungal Genet. Biol.* **2016**, 96, 33–46.
25. Coca-Ruiz, V.; García-Barba, A.; Ale, J.; Collado, I.G. Loss of a major toxin gene cluster defines metabolic divergence and host-specific virulence in *Botrytis pseudocinerea*. *PLOS ONE* **2026**, 21, e0339017.
26. ten Have, A.; Mulder, W.; Visser, J.; van Kan, J.A. The endopolygalacturonase gene *Bcpg1* is required for full virulence of *Botrytis cinerea*. *Mol. Plant-Microbe Interact.* **1998**, 11, 1009–1016.
27. Blanco-Ulate, B.; Morales-Cruz, A.; Amrine, K.C.; Labavitch, J.M.; Powell, A.L.; Cantu, D. Genome-wide transcriptional profiling of *Botrytis cinerea* genes targeting plant cell walls during host infection. *Front. Plant Sci.* **2014**, 5, 435.
28. Cheung, N.; Tian, L.; Liu, X. The destructive fungal pathogen *Botrytis cinerea*—insights from genes studied with mutant analysis. *Pathogens* **2020**, 9, 923.
29. Ma, L.; Liu, T.; Zhang, K.; Lu, Y.; Chen, X. *Botrytis cinerea* transcription factor BcXyr1 regulates (hemi-)cellulase production and fungal virulence. *mSystems* **2022**, 7, e01042-22.

30. Canessa, P.; Schumacher, J.; Hevia, M.A.; Tudzynski, P.; Larrondo, L.F. Assessing the effects of light on differentiation and virulence of the plant pathogen *Botrytis cinerea*: characterization of the White Collar Complex. *PLOS ONE* **2013**, 8, e84223.
31. Schumacher, J.; Simon, A.; Cohrs, K.C.; Viaud, M.; Tudzynski, P. The transcription factor BcLTF1 regulates virulence and light responses in the necrotrophic plant pathogen *Botrytis cinerea*. *PLOS Genet.* **2014**, 10, e1004040.
32. Cohrs, K.C.; Schumacher, J. The two cryptochrome/photolyase family proteins fulfill distinct roles in DNA photorepair and regulation of conidiation in *Botrytis cinerea*. *Appl. Environ. Microbiol.* **2017**, 83, e00812-17.
33. López-Cruz, J.; Sánchez Ó.; Cortés, E.; Alfaro, P.; Barriuso C. Absence of Cu-Zn superoxide dismutase BcSod1 reduces *Botrytis cinerea* virulence in *Arabidopsis thaliana* and tomato plants, revealing interplay among reactive oxygen species, callose and signalling pathways. *Mol. Plant Pathol.* **2017**, 18, 16–31.
34. Xu, Y.Q.; Tong, Z.; Zhang, X.; Luo, Z.; Shao, W.; Li, L.; Ma, Q.; Zheng, X.; Fang, W.Y. Plant volatile organic compound (E)-2-hexenal facilitates *Botrytis cinerea* infection of fruits by inducing sulfate assimilation. *New Phytol.* **2021**, 231, 432–446.
35. Rolke, Y.; Liu, S.; Quidde, T. Functional analysis of H_2O_2-generating systems in *Botrytis cinerea*: the major Cu-Zn-superoxide dismutase BcSod1 contributes to virulence on French bean, whereas a glucose oxidase BcGox1 is dispensable. *Mol. Plant Pathol.* **2004**, 5, 17–27.
36. Yuan, X.; Yang, F.; Wang, Y. Scopoletin negatively regulates the HOG signalling pathway and inhibits infection structures of *Botrytis cinerea*. *Phytopathol. Res.* **2024**, 6, 1.
37. Li, H.; Zhang, Z.Q.; Li, B.Q.; Qin, G.Z.; Tian, S.P. Actin is required for cellular development and virulence of *Botrytis cinerea* via the mediation of secretory proteins. *mSystems* **2020**, 5, e00732-19.

548 38. Rascle, C.; Billon-Grand, G.; Poussereau, N. Validation of reference genes for
549 quantitative RT-PCR normalization in *Botrytis cinerea*. *J. Microbiol. Methods*
550 **2017**, 139, 10–17.
551 39. Kokkelink, L.; Minz, A.; Al-Masri, M. The small GTPase BcCdc42 affects
552 nuclear division, germination and virulence of the gray mold fungus *Botrytis*
553 *cinerea*. *Fungal Genet. Biol.* **2011**, 48, 1012–1019.
554 40. Soulié, M.C.; Piffeteau, A.; Choquer, M.; Boccara, M.; Vidal-Cros, A. Disruption
555 of *BcCHS1* class I chitin synthase gene results in weakened cell wall and reduced
556 virulence of *Botrytis cinerea*. *Fungal Genet. Biol.* **2003**, 40, 38–46.
557 41. Gebremichael, S.; Ciofini, A. Exogenous dsRNAs targeting chitin and glucan
558 synthase genes inhibit growth and virulence of *Botrytis cinerea*. *Pest Manag. Sci.*
559 **2023**, 79, 3012–3022.
560 42. Li, J.; Guo, C.; Wen, X.; Chen, H.; Du, H.; Liu, D. Chemical composition of
561 *Artemisia argyi* essential oil and its antifungal activity against *Botrytis cinerea*
562 via oxidative damage. *J. Ethnopharmacol.* **2024**, 331, 118344.
563 43. Chen, L.; Wang, X.; Liu, J. Investigating the action model of resistance
564 enhancement induced by bacterial volatile organic compounds against *Botrytis*
565 *cinerea* in tomato fruit. *Front. Plant Sci.* **2024**, 14, 1475416.
566 44. Cui, K.; Zhao, Y.; He, L. Comparison of transcriptome profiles of the fungus
567 *Botrytis cinerea* and insect pest *Bradysia odoriphaga* in response to
568 benzothiazole. *Front. Microbiol.* **2020**, 11, 1043.
569 45. Yang, J.; Zheng, Y. Antifungal activity of paeonol against *Botrytis cinerea* via
570 disrupting fungal membrane integrity. *Front. Microbiol.* **2024**, 15, 1509124.
571 46. Wu, Z.; Li, Y.; Wang, H. Multidrug resistance of *Botrytis cinerea* associated with
572 its adaptation to plant secondary metabolites. *mBio* **2024**, 15, e02237-23.
573 47. Zhang, J.; Ma, S.; Du, S. Antifungal activities of thymol and carvacrol against
574 postharvest grey mould pathogen *Botrytis cinerea*. *J. Food Sci. Technol.* **2019**, 56,
575 641–680.
576 48. Tian, S.P. Molecular basis of pathogenicity of postharvest pathogenic fungi and
577 control strategy in fruits. *Mol. Hortic.* **2022**, 2, 1–18.

49. Sofianos, G.; Samaras, A.; Karaoglanidis, G. Multiple and multidrug resistance in *Botrytis cinerea*: molecular mechanisms of MLR/MDR strains. *Front. Plant Sci.* **2023**, 14, 1273193.
50. Pinedo, C.; Collado, I.G. Biosynthesis of the sesquiterpene botrydial in *Botrytis cinerea*: mechanism and stereochemistry of the enzymatic formation of presilphiperfolan-8β-ol. *J. Am. Chem. Soc.* **2009**, 131, 11336–11346.
51. Viefhues, A.; Heller, J.; Temme, N. Redox systems in *Botrytis cinerea*: impact on fungal development and virulence. *Mol. Plant-Microbe Interact.* **2014**, 27, 858–874.
52. Duanis-Assaf, D. Double-stranded RNA targeting ergosterol biosynthesis pathway controls *Botrytis cinerea* and postharvest grey mould. *Plant Biotechnol. J.* **2022**, 20, 226–237.
53. Roberts, A.; Trapnell, C.; Donaghey, J.; Rinn, J.L.; Pachter, L. Improving RNA-Seq expression estimates by correcting for fragment bias. *Genome Biol.* **2011**, 12, R22.
54. Trapnell, C.; Williams, B.A.; Pertea, G.; Mortazavi, A.; Kwan, G.; van Baren, M.J.; Salzberg, S.L.; Wold, B.J.; Pachter, L. Transcript assembly and quantification by RNA-Seq reveals unannotated transcripts and isoform switching during cell differentiation. *Nat. Biotechnol.* **2010**, 28, 511–515.
55. Langmead, B.; Salzberg, S.L. Fast gapped-read alignment with Bowtie 2. *Nat. Methods* **2012**, 9, 357–359.
56. Roberts, A.; Pachter, L. Streaming fragment assignment for real-time analysis of sequencing experiments. *Nat. Methods* **2013**, 10, 71–73.
57. Nishida, E.; Gotoh, Y. The MAP kinase cascade is essential for diverse signal transduction pathways. *Trends Biochem. Sci.* **1993**, 18, 128–131.
58. Dickman, M.B.; Yarden, O. Serine/threonine protein kinases and phosphatases in filamentous fungi. *Fungal Genet. Biol.* **1999**, 26, 99–117.

Figure legends.

Figure 1. Global transcriptome profiling of *B. cinerea* under L-carvone fumigation. (A) Boxplot of normalized gene expression distribution across all samples. (B) Sample correlation heatmap. (C) PCA score plot of transcriptional profiles; red dots represent BCCK group, blue dots represent BCEC group. (D) Volcano plot of DEGs; red dots = significantly upregulated genes, blue dots = significantly downregulated genes, gray dots = non-significant genes.

Figure 2. Hierarchical clustering heatmap of all DEGs. Red indicates upregulated transcripts, green indicates downregulated transcripts.

Figure 3. KEGG pathway enrichment of DEGs. (A) Enrichment results of significantly upregulated DEGs. (B) Enrichment results of significantly downregulated DEGs.

Figure 4. GO functional enrichment of DEGs. (A) GO enrichment for upregulated DEGs. (B) GO enrichment for downregulated DEGs.

Figure 5. Classification of all detected metabolites in *B. cinerea*.

Figure 6. Metabolomic shifts of *B. cinerea* induced by L-carvone fumigation. (A) PCA score plot of metabolome data; pink = BCEC treatment group, blue = BCCK control group. (B) OPLS-DA score plot; pink = BCEC treatment group, blue = BCCK control group.

Figure 7. Screening and hierarchical clustering of DAMs. (A) Volcano plot of DAMs; red = upregulated DAMs, green = downregulated DAMs, gray = non-significant metabolites. (B) Hierarchical clustering heatmap of DAMs; green corresponds to BCEC group, red corresponds to BCCK group.

Figure 8. KEGG pathway enrichment analysis of significantly differential abundant metabolites.

Figure S1. Sequencing saturation curves of transcriptome data. (A–C) Biological replicates of BCCK group; (D–F) Biological replicates of BCEC group.

Figure S2. Overlapped total ion chromatograms (TICs) of QC samples for metabolome analysis.

Table Captions

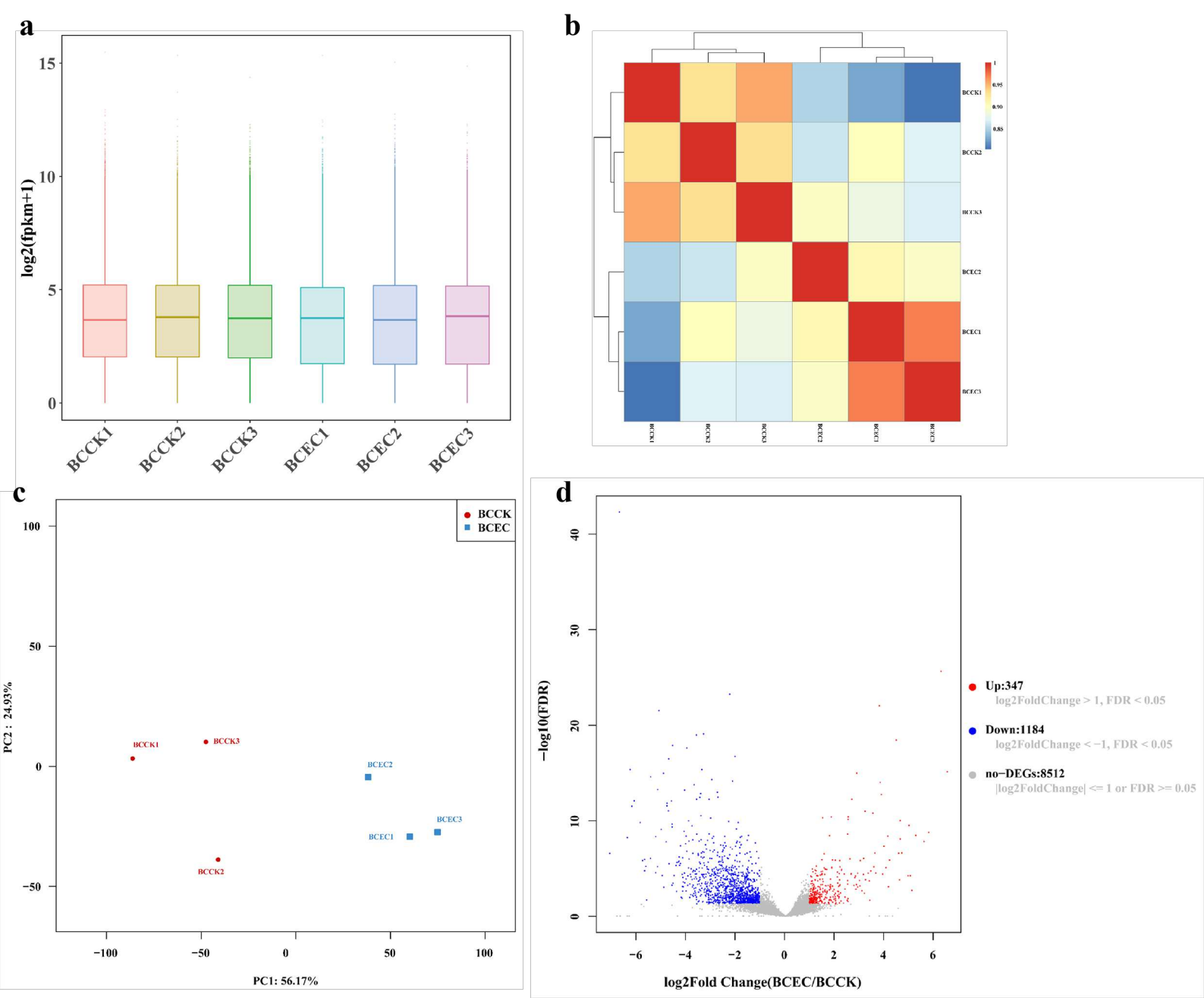
Table 1. Summary statistics of RNA-seq sequencing data.

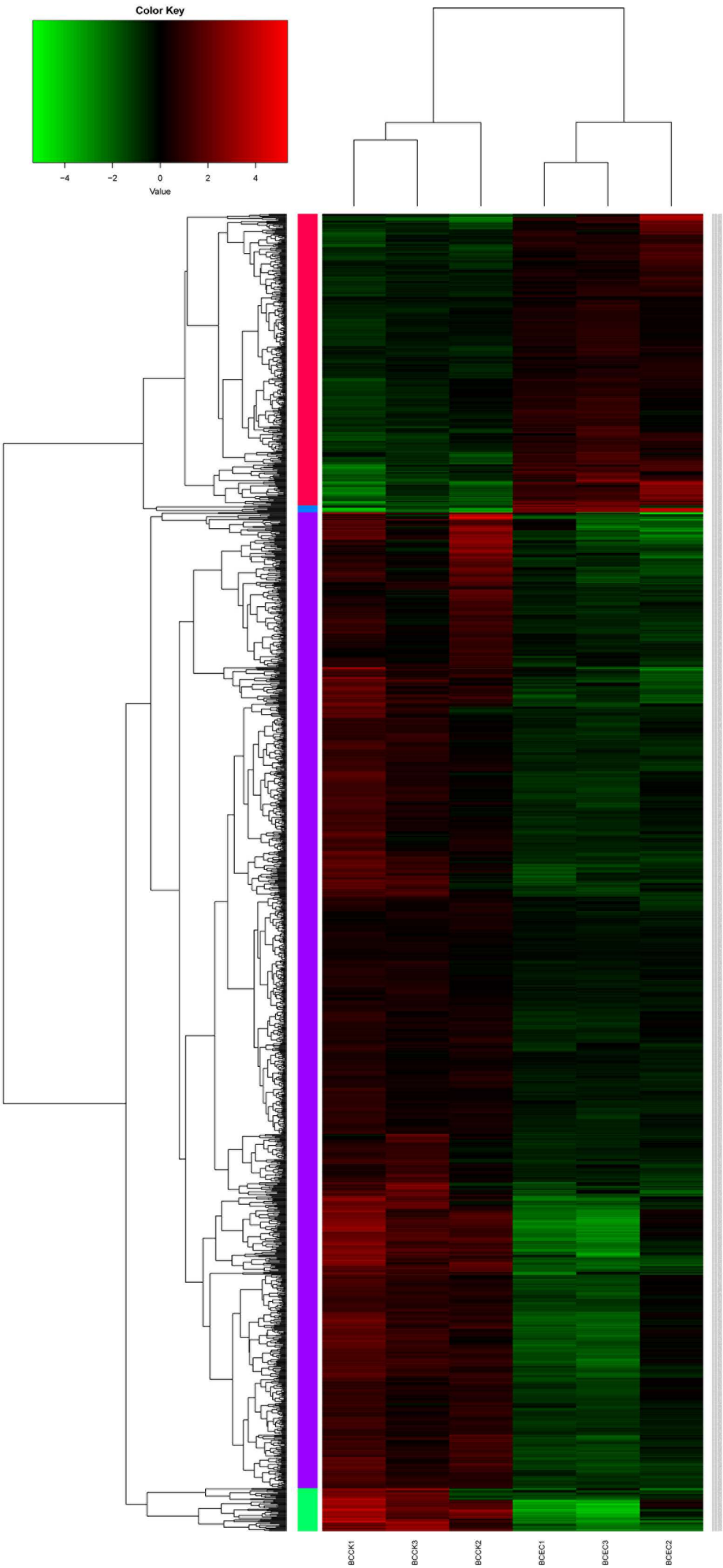
Table 2. List of key significantly differentially expressed genes.

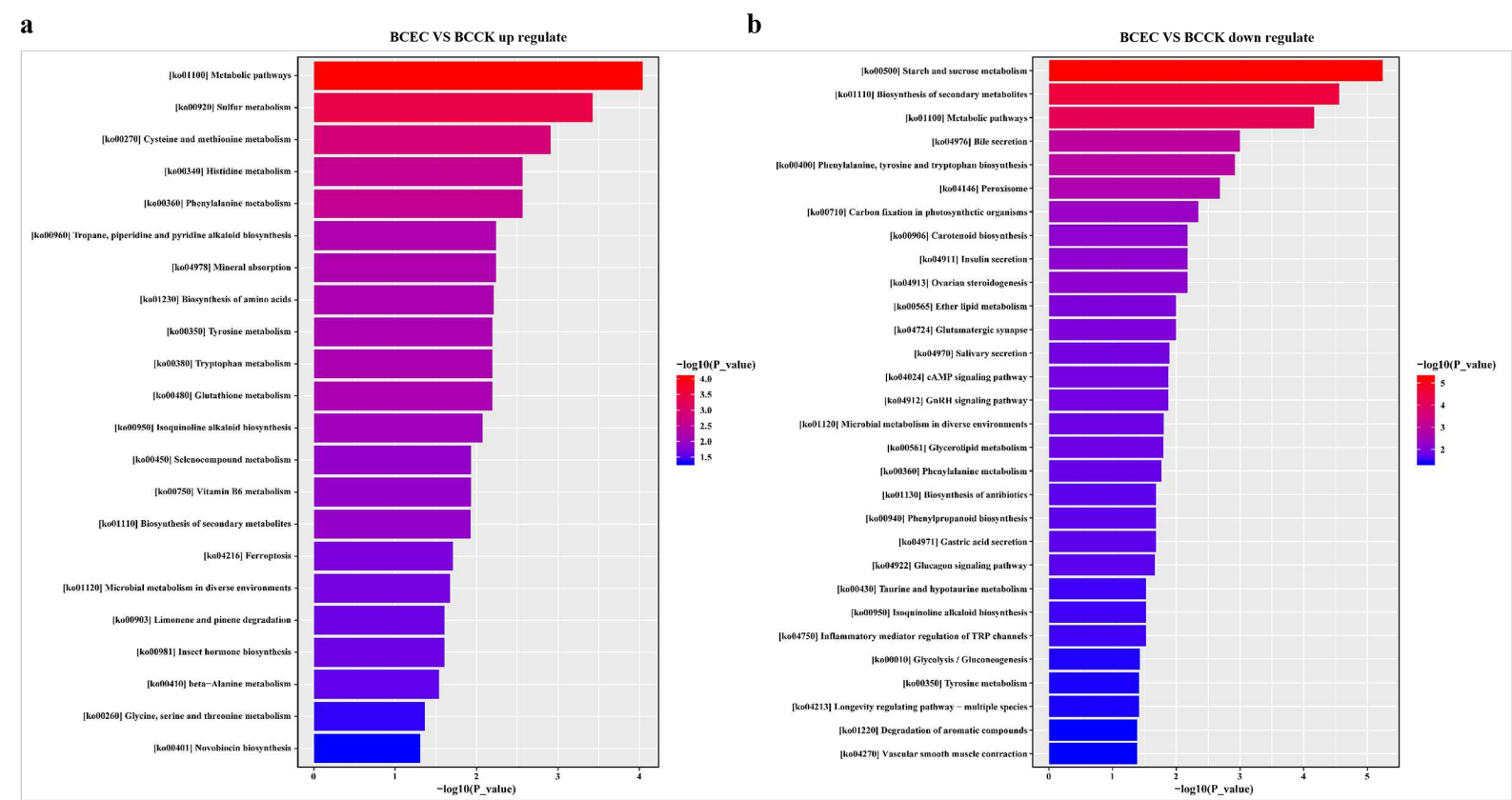
Table 3. List of key significantly differential abundant metabolites.

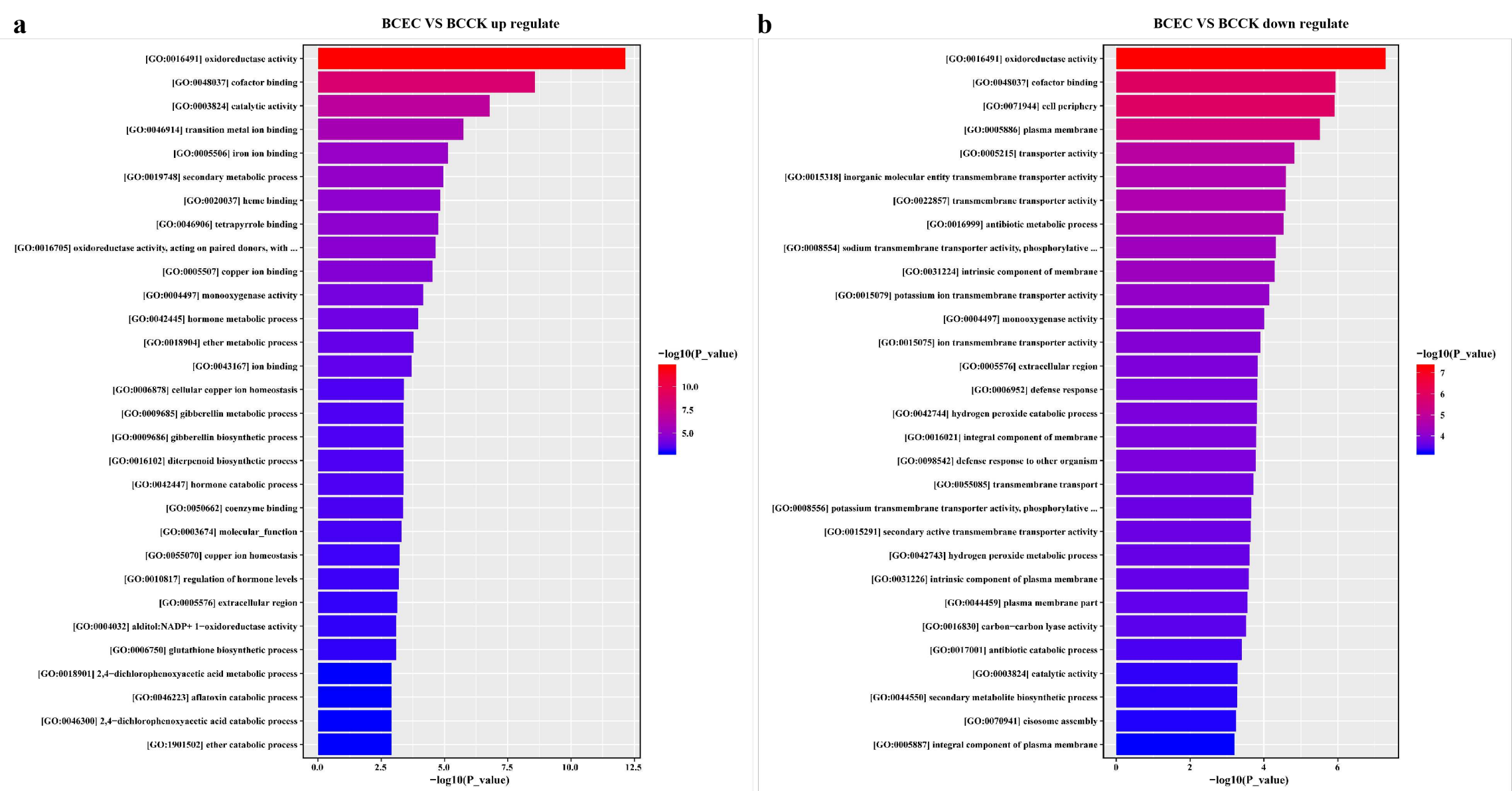
Table S1. List of significantly differentially expressed genes between BCCK and BCEC groups.

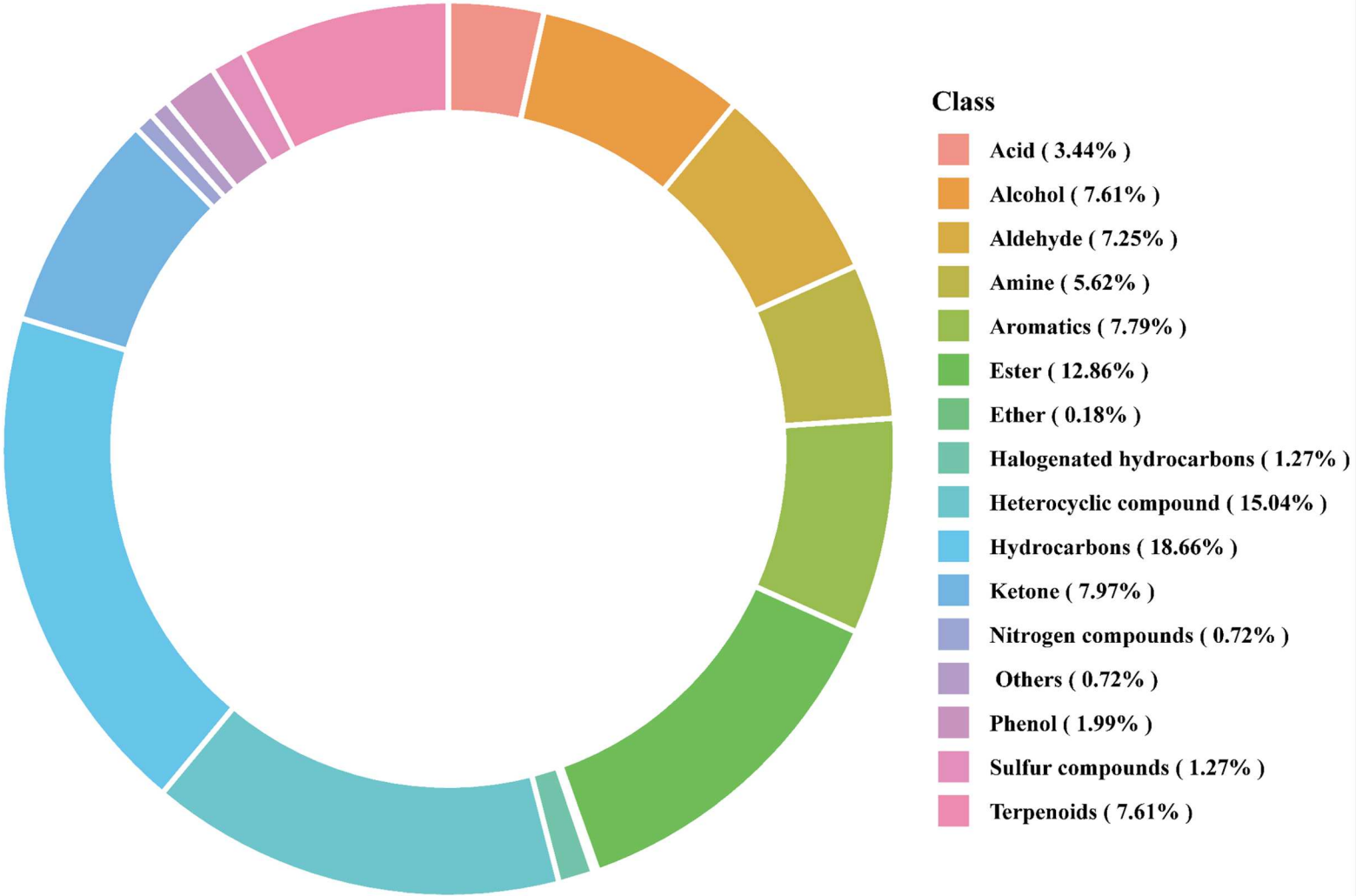
Table S2. List of significantly differential abundant metabolites between BCCK and BCEC groups.

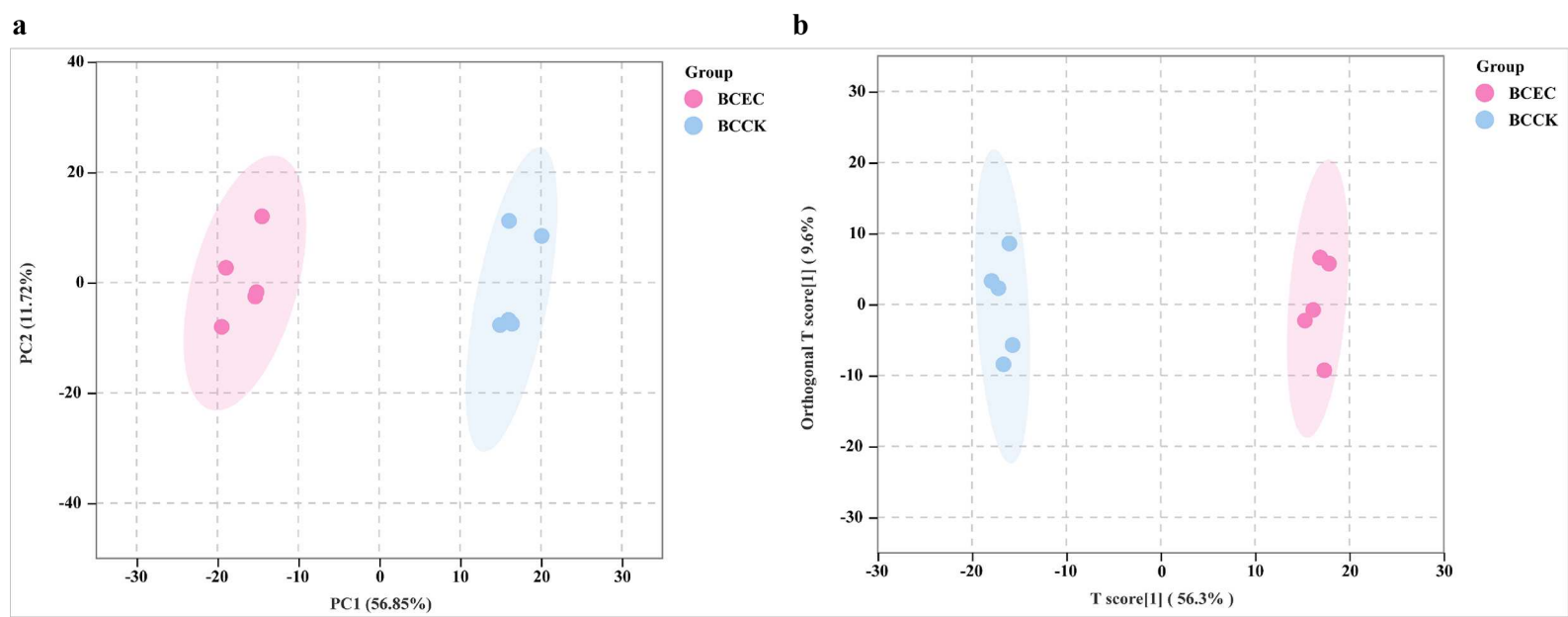

a
log2(fpkm+1)
15
10
5
0
BCCK1
BCCK2
BCCK3
BCEC1
BCEC2
BCEC3
b
1
0.95
0.90
0.85
BCCK1
BCCK2
BCCK3
BCEC2
BCEC1
BCEC3
c
BCCK
BCEC
PC2 : 24.93%
PC1: 56.17%
100
50
0
−50
−100
BCCK1
BCCK3
BCCK2
BCEC2
BCEC3
BCEC1
d
−log10(FDR)
log2Fold Change(BCEC/BCCK)
40
30
20
10
0
−6
−4
−2
0
2
4
6
Up:347
log2FoldChange > 1, FDR < 0.05
Down:1184
log2FoldChange < −1, FDR < 0.05
no−DEGs:8512
|log2FoldChange| <= 1 or FDR >= 0.05

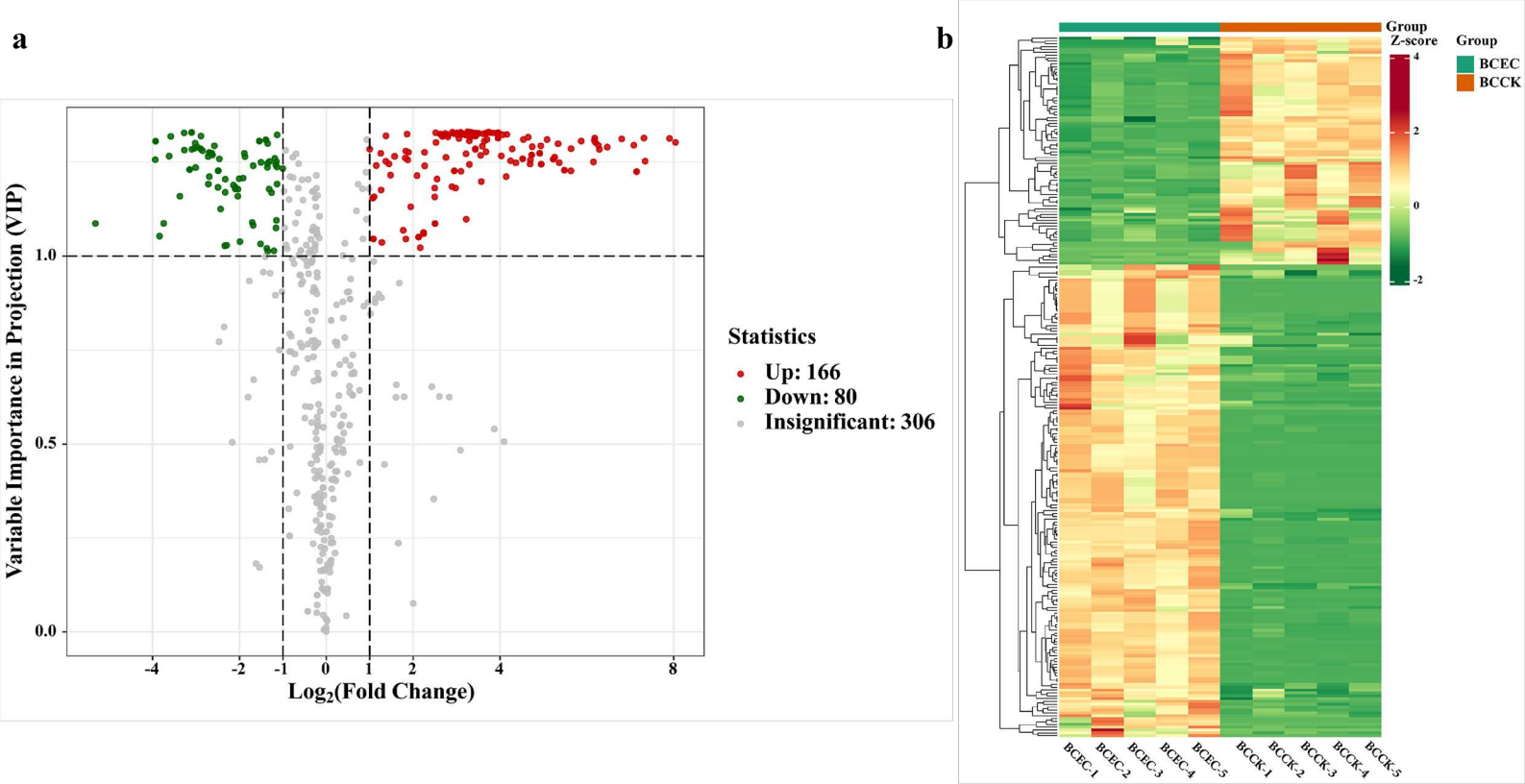

Color Key
−4
−2
0
2
4
Value
BCCK1
BCCK3
BCCK2
BCEC1
BCEC3
BCEC2


a
BCEC VS BCCK up regulate
[ko01100] Metabolic pathways
[ko00920] Sulfur metabolism
[ko00270] Cysteine and methionine metabolism
[ko00340] Histidine metabolism
[ko00360] Phenylalanine metabolism
[ko00960] Tropane, piperidine and pyridine alkaloid biosynthesis
[ko04978] Mineral absorption
[ko01230] Biosynthesis of amino acids
[ko00350] Tyrosine metabolism
[ko00380] Tryptophan metabolism
[ko00480] Glutathione metabolism
[ko00950] Isoquinoline alkaloid biosynthesis
[ko00450] Selenocompound metabolism
[ko00750] Vitamin B6 metabolism
[ko01110] Biosynthesis of secondary metabolites
[ko04216] Ferroptosis
[ko01120] Microbial metabolism in diverse environments
[ko00903] Limonene and pinene degradation
[ko00981] Insect hormone biosynthesis
[ko00410] beta-Alanine metabolism
[ko00260] Glycine, serine and threonine metabolism
[ko00401] Novobiocin biosynthesis
0
1
2
3
4
−log10(P_value)
−log10(P_value)
4.0
3.5
3.0
2.5
2.0
1.5
b
BCEC VS BCCK down regulate
[ko00500] Starch and sucrose metabolism
[ko01110] Biosynthesis of secondary metabolites
[ko01100] Metabolic pathways
[ko04976] Bile secretion
[ko00400] Phenylalanine, tyrosine and tryptophan biosynthesis
[ko04146] Peroxisome
[ko00710] Carbon fixation in photosynthetic organisms
[ko00906] Carotenoid biosynthesis
[ko04911] Insulin secretion
[ko04913] Ovarian steroidogenesis
[ko00565] Ether lipid metabolism
[ko04724] Glutamatergic synapse
[ko04970] Salivary secretion
[ko04024] cAMP signaling pathway
[ko04912] GnRH signaling pathway
[ko01120] Microbial metabolism in diverse environments
[ko00561] Glycerolipid metabolism
[ko00360] Phenylalanine metabolism
[ko01130] Biosynthesis of antibiotics
[ko00940] Phenylpropanoid biosynthesis
[ko04971] Gastric acid secretion
[ko04922] Glucagon signaling pathway
[ko00430] Taurine and hypotaurine metabolism
[ko00950] Isoquinoline alkaloid biosynthesis
[ko04750] Inflammatory mediator regulation of TRP channels
[ko00010] Glycolysis / Gluconeogenesis
[ko00350] Tyrosine metabolism
[ko04213] Longevity regulating pathway - multiple species
[ko01220] Degradation of aromatic compounds
[ko04270] Vascular smooth muscle contraction
0
1
2
3
4
5
−log10(P_value)
−log10(P_value)
5
4
3
2


a
BCEC VS BCCK up regulate
[GO:0016491] oxidoreductase activity
[GO:0048037] cofactor binding
[GO:0003824] catalytic activity
[GO:0046914] transition metal ion binding
[GO:0005506] iron ion binding
[GO:0019748] secondary metabolic process
[GO:0020037] heme binding
[GO:0046906] tetrapyrrole binding
[GO:0016705] oxidoreductase activity, acting on paired donors, with ...
[GO:0005507] copper ion binding
[GO:0004497] monooxygenase activity
[GO:0042445] hormone metabolic process
[GO:0018904] ether metabolic process
[GO:0043167] ion binding
[GO:0006878] cellular copper ion homeostasis
[GO:0009685] gibberellin metabolic process
[GO:0009686] gibberellin biosynthetic process
[GO:0016102] diterpenoid biosynthetic process
[GO:0042447] hormone catabolic process
[GO:0050662] coenzyme binding
[GO:0003674] molecular_function
[GO:0055070] copper ion homeostasis
[GO:0010817] regulation of hormone levels
[GO:0005576] extracellular region
[GO:0004032] alditol:NADP+ 1−oxidoreductase activity
[GO:0006750] glutathione biosynthetic process
[GO:0018901] 2,4−dichlorophenoxyacetic acid metabolic process
[GO:0046223] aflatoxin catabolic process
[GO:0046300] 2,4−dichlorophenoxyacetic acid catabolic process
[GO:1901502] ether catabolic process
0.0
2.5
5.0
7.5
10.0
12.5
−log10(P_value)
−log10(P_value)
10.0
7.5
5.0
b
BCEC VS BCCK down regulate
[GO:0016491] oxidoreductase activity
[GO:0048037] cofactor binding
[GO:0071944] cell periphery
[GO:0005886] plasma membrane
[GO:0005215] transporter activity
[GO:0015318] inorganic molecular entity transmembrane transporter activity
[GO:0022857] transmembrane transporter activity
[GO:0016999] antibiotic metabolic process
[GO:0008554] sodium transmembrane transporter activity, phosphorylative ...
[GO:0031224] intrinsic component of membrane
[GO:0015079] potassium ion transmembrane transporter activity
[GO:0004497] monooxygenase activity
[GO:0015075] ion transmembrane transporter activity
[GO:0005576] extracellular region
[GO:0006952] defense response
[GO:0042744] hydrogen peroxide catabolic process
[GO:0016021] integral component of membrane
[GO:0098542] defense response to other organism
[GO:0055085] transmembrane transport
[GO:0008556] potassium transmembrane transporter activity, phosphorylative ...
[GO:0015291] secondary active transmembrane transporter activity
[GO:0042743] hydrogen peroxide metabolic process
[GO:0031226] intrinsic component of plasma membrane
[GO:0044459] plasma membrane part
[GO:0016830] carbon−carbon lyase activity
[GO:0017001] antibiotic catabolic process
[GO:0003824] catalytic activity
[GO:0044550] secondary metabolite biosynthetic process
[GO:0070941] eisosome assembly
[GO:0005887] integral component of plasma membrane
0
2
4
6
−log10(P_value)
−log10(P_value)
7
6
5
4


Class
Acid (3.44%)
Alcohol (7.61%)
Aldehyde (7.25%)
Amine (5.62%)
Aromatics (7.79%)
Ester (12.86%)
Ether (0.18%)
Halogenated hydrocarbons (1.27%)
Heterocyclic compound (15.04%)
Hydrocarbons (18.66%)
Ketone (7.97%)
Nitrogen compounds (0.72%)
Others (0.72%)
Phenol (1.99%)
Sulfur compounds (1.27%)
Terpenoids (7.61%)


a
b
Group
BCEC
BCCK
PC1 (56.85%)
PC2 (11.72%)
T score[1] (56.3%)
Orthogonal T score[1] (9.6%)


a
b
Variable Importance in Projection (VIP)
1.0
0.5
0.0
-4
-2
-1
0
1
2
4
8
Log2(Fold Change)
Statistics
Up: 166
Down: 80
Insignificant: 306
Group
Z-score
4
2
0
-2
Group
BCEC
BCCK
BCEC-1
BCEC-2
BCEC-3
BCEC-4
BCEC-5
BCCK-1
BCCK-2
BCCK-3
BCCK-4
BCCK-5

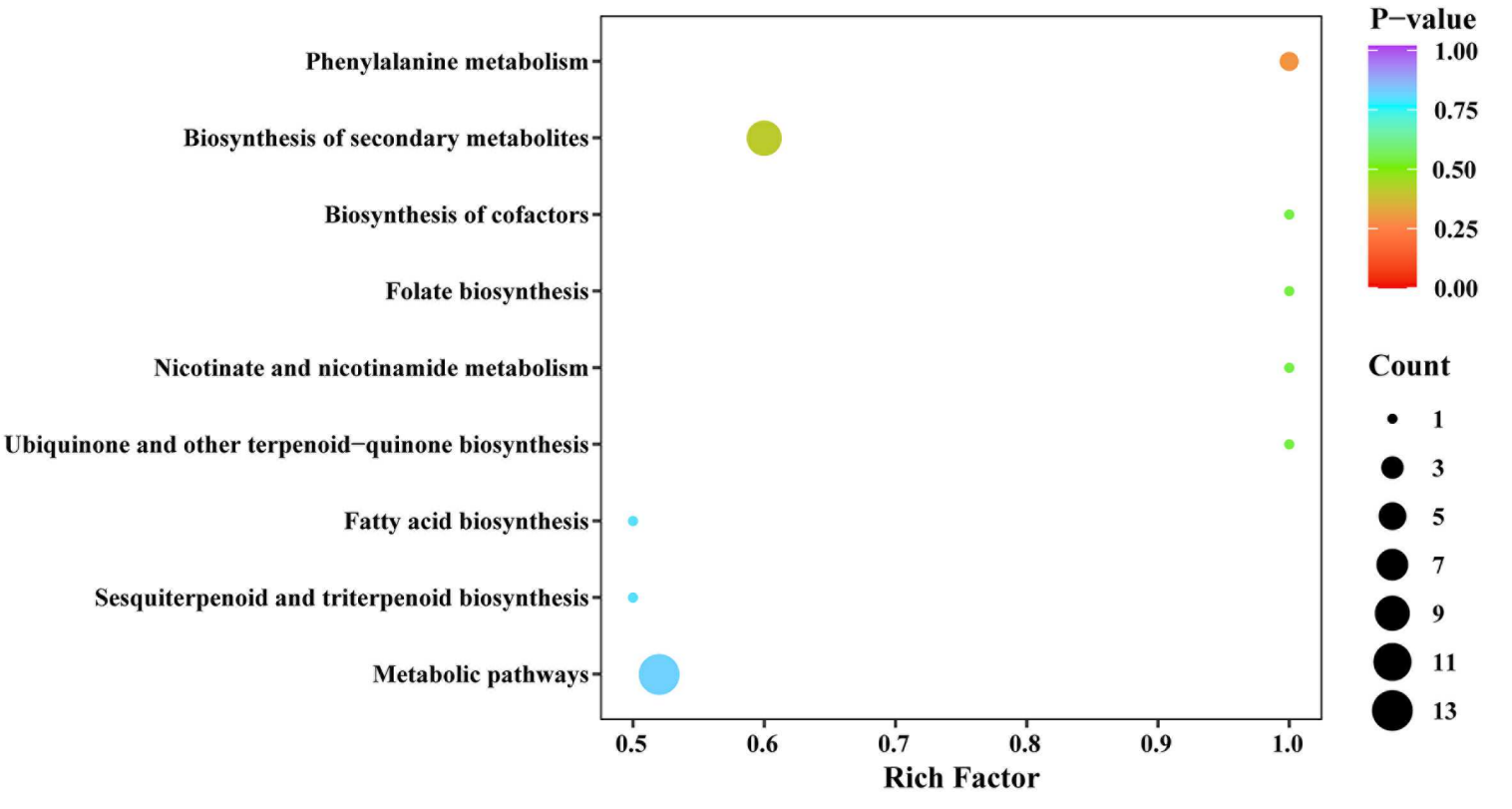

Phenylalanine metabolism
Biosynthesis of secondary metabolites
Biosynthesis of cofactors
Folate biosynthesis
Nicotinate and nicotinamide metabolism
Ubiquinone and other terpenoid−quinone biosynthesis
Fatty acid biosynthesis
Sesquiterpenoid and triterpenoid biosynthesis
Metabolic pathways
0.5
0.6
0.7
0.8
0.9
1.0
Rich Factor
P−value
1.00
0.75
0.50
0.25
0.00
Count
1
3
5
7
9
11
13

Table 1. Summary statistics of RNA-seq sequencing data.

Samples	Clean reads	Clean bases	Error rates %	Total mapped	Q30 %	GC %	Gene Numbers
BCCK1	85.05 Mb	12.21 Gb	0.03	96.21%	93.38	47.63	13,166
BCCK2	78.72 Mb	11.41 Gb	0.03	96.22%	93.24	46.74	13,337
BCCK3	72.62 Mb	10.60 Gb	0.03	96.00%	93.35	47.55	13,094
BCEC1	87.97 Mb	12.75 Gb	0.03	96.53%	93.41	47.19	13,258
BCEC2	76.51 Mb	11.13 Gb	0.03	96.34%	93.50	47.84	12,724
BCEC3	80.24 Mb	11.57 Gb	0.03	96.38%	93.43	47.07	13,203

Table 2. List of key significantly differentially expressed genes

	Gene_id	Name	Regulate	Significant
Toxin related	*gene-BCIN_01g00140*	*BcBOT6*	down	yes
	gene-BCIN_01g00150	*BcBOT2*	down	yes
	gene-BCIN_01g00160	*BcBOT1*	down	yes
	gene-BCIN_01g02510	*Bcpg1*	down	yes
	gene-BCIN_01g02520	*Bcpg2*	down	yes
	gene-BCIN_01g02710	*Bccel1*	down	yes
	gene-BCIN_01g03010	*Bccon1*	down	yes
	gene-BCIN_01g03020	*Bccon2*	down	yes
Damage repair	*gene-BCIN_01g01450*	*BcatrO*	Up	yes
	gene-BCIN_01g04230	*Bcmet16*	down	yes
	gene-BCIN_01g04240	*BcGCL*	down	yes
	gene-BCIN_01g04250	*BcGPX*	down	yes
	gene-BCIN_01g02150	*BcSOD1*	UP	yes
	gene-BCIN_01g02160	*BcCAT1*	UP	yes
	gene-BCIN_01g03890	*BcGST1*	UP	yes
Growth related	*gene-BCIN_01g00210*	*BcERG7*	down	yes
	gene-BCIN_01g00220	*BcERG12*	down	yes
	gene-BCIN_01g00230	*BcERG27*	down	yes
	gene-BCIN_01g00310	*BcFAS1*	down	yes
	gene-BCIN_01g02010	*BcactA*	down	yes
	gene-BCIN_01g02020	*BcTUB1*	down	yes
	gene-BCIN_01g02030	*BcCDC42*	down	yes

Table 3. List of key significantly differential abundant metabolites

	代谢物	Regulate	Significant
Toxin related	(2E,4Z)-2,4-Decadienal	down	yes
	(E)-2-Octenal	down	yes
	Benzothiazole	down	yes
	4-hydroxy-Benzoic Acid	down	yes
	Benzeneacetic acid	down	yes
	Decanal	down	yes
	γ-Cadinene	down	yes
Damage repair	Carvacrol	UP	yes
	Camphene	down	yes
	1-methyl-4-(1-methylethylidene)-Cyclohexanol	UP	yes
	Dipropyl disulfide	UP	yes
	(1-methylethylidene)-Cyclohexane	UP	yes
Growth related	3,7,7-trimethyl-Bicyclo[4.1.0]heptane	down	yes
	(2,2,6-Trimethyl-bicyclo[4.1.0])-methanol	down	yes
	1,2,3,5-tetramethyl-Benzene	down	yes
	Biphenyl	UP	yes

Supplementary Files

This is a list of supplementary files associated with this preprint. Click to download.

- TableS1.xlsx
- TableS2.xlsx
- Fig.S1.tif